

Date of publication xxxx 00, 0000, date of current version xxxx 00, 0000.

Digital Object Identifier 10.1109/ACCESS.2023.DOI

A Single Phase Hybrid Multiport Microinverter for Photovoltaic Energy Controlled by Exact Linearization

RODRIGO ALIAGA¹, (Student Member, IEEE), Javier Muñoz¹, (Member, IEEE), MARCO RIVERA¹, (SENIOR MEMBER, IEEE), PATRICK WHEELER², (FELLOW MEMBER, IEEE), JAIME ROHTEN³, AND ANDREW TRENTIN²

¹Department of Electrical Engineering, Universidad de Talca, Camino Los Niches Km. 1, Curicó, 3340000, Chile.

²Department of Electrical and Electronic Engineering, University Park, University of Nottingham, NG7 2RD, UK

³Department of Electrical and Electronic Engineering, Universidad del Bío-Bío, Av. Collao 1202, Región del Bío-Bío 4051381, Chile.

Corresponding author: Marco R. Author (e-mail: marcoriv@utalca.cl).

ABSTRACT Solar energy can be captured by Photovoltaics (PV) and converted into electrical power. This electrical power can then be connected to grids by power electronic converters, which can also operate the PV panels at around their maximum power point (MPP), maximizing the harvested energy. When the PV panels are connected in an array, the partial shading effect generates a distortion of the power curve can result in a power loss since tracking algorithms might not be able to detect the MPP. To solve this issue microinverters have been proposed, with a small power electronic converter being connected to each PV panel, this arrangement enables independence for maximum power point tracking and electrical isolation. This paper presents a double output multiport microinverter capable of feeding DC and AC loads or providing connection to a single-phase AC grid and energy storage. The proposed structure can be operated in grid-connected and islanded modes. This paper describes the microinverter controlled with the exact linearization technique on both the DC and AC sides, obtaining a lineal transfer function representation of the nonlinear and coupled power electronic converters. The operation of the proposed topology and its control strategy is validated using a laboratory proof-of-concept prototype.

INDEX TERMS Exact Linearization; Microinverter; Multiport.

I. INTRODUCTION

The proliferation in the use of renewable energy sources has led to the investigation of large scale renewable energy systems, as well as in microgrids and residential use. Thus, microinverters are an interesting way to extract and inject power into the AC mains, whilst, tracking the maximum power point (MPP) even under partial shading conditions. This consists of a photovoltaic (PV) power curve distortion, as a result of the by-pass diodes, conduction [1], when a group of cells is shaded [2]. These diodes, connected in parallel to the group of cells in the Photovoltaic (PV) module are fundamental, and cannot be omitted, because they prevent hot spots and consequently a PV module damage [3], since the PV cell is prevented from acting as an electrical load. However, the consequence of using By-pass diodes is the appearance of Local Maximum Power Points (LMPP) and a Global Maximum Power Point (GMPP) [4]. In fact, Figure

1, shows a comparison, where the characteristic PV power curve has only one MPP for standard conditions (Figure 1 a)), while the distorted PV power curve presents a local and global MPP with the presence of partial shading. It is possible to see from Figure 1 b) a power loss of around 30 percent if the MPPT algorithm erroneously selects the LMPP as the GMPP.

The output of the MPPT algorithm is the reference to the power electronics converter, which can be the PV voltage or current. In technical literature, four large groups of MPPT algorithms are reported: classic, intelligent, optimized, and hybrid, which vary in their complexity, efficiency, and effectiveness. The article in [5] presents a complete review of tracking methods, while works, such as [6], study techniques using hardware to scan the power curve and thus ensure the optimal operating point.

Microinverters [7], [8] are capable of addressing the shad-

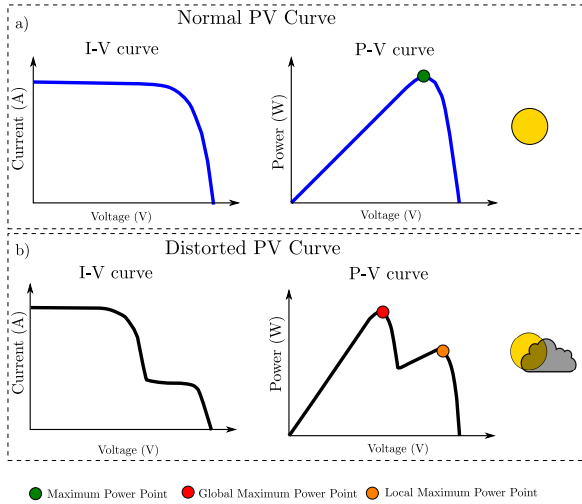


FIGURE 1: PV power curve, a) a normal PV curve, b) a string with multiple power points.

owing effect mentioned above, as described in [9], where a complete review of topologies is presented. Usually, the microinverters are divided into two main types; isolated [10] and non-isolated [11]. Isolated topologies are characterized by the quality of energy transmitted with low noise and reduced electromagnetic interference. Non-isolated topologies are distinguished by simplicity, with a reduced number of components [12]. Regarding multiport converters, these are widely used in industries such as aviation, where it is necessary to supply different types of loads, either in a DC or AC voltage. The work in [13] presents a multiport conversion system for electric aircraft. Meanwhile in PV energy, hybrid systems have been developed with different operation modes, either disconnected or connected to the electrical grid. Moreover, they have the ability to store energy in a battery [14].

Regarding control strategies for such microinverter structures, they can be divided into five large groups: hysteresis, linear control, sliding mode, predictive, and artificial intelligence. Within these groups, current control by hysteresis band can be highlighted, since it is an obvious choice with its easy implementation. However, it has a disadvantage: the steady state error [15], [16]. On the other hand, the classic PI control is widely used in linear systems or for controlling around a fixed reference point. The current and voltage control based on sliding mode makes it possible for good performance under operating point changes and modeling uncertainties [17]; nevertheless, it presents the existence of chattering [18]. Regarding predictive control, this stands out for being a non-linear control with great ease of implementation [19], but with a large computational burden added to the existence of error in a steady state. Finally, the fuzzy control [20] is an advanced control for which there is no mathematical analysis that guarantees the existence of zero error in a steady state and also needs an expert to tune the control parameters.

This paper proposes the use of the exact linearization technique, which basically, consists of introducing a transformation at the input of the system [21], [22] aimed to achieve a linear system between the input and output. This transformation is made using mathematical operations among the system variables such as voltages or currents. This work is focused on presenting a hybrid multiport microinverter (HMM) capable of supplying DC and AC loads, energy storage in a battery bank, and injecting energy into the electrical grid. The entire system is controlled using a strategy based on multiloops with simple and double exact linearization plus power balance. The novelty of this work lies in the fact that a highly complex nonlinear system is converted into a simple system to be controlled. Furthermore, input voltage disturbances are canceled, and the converter may operate in

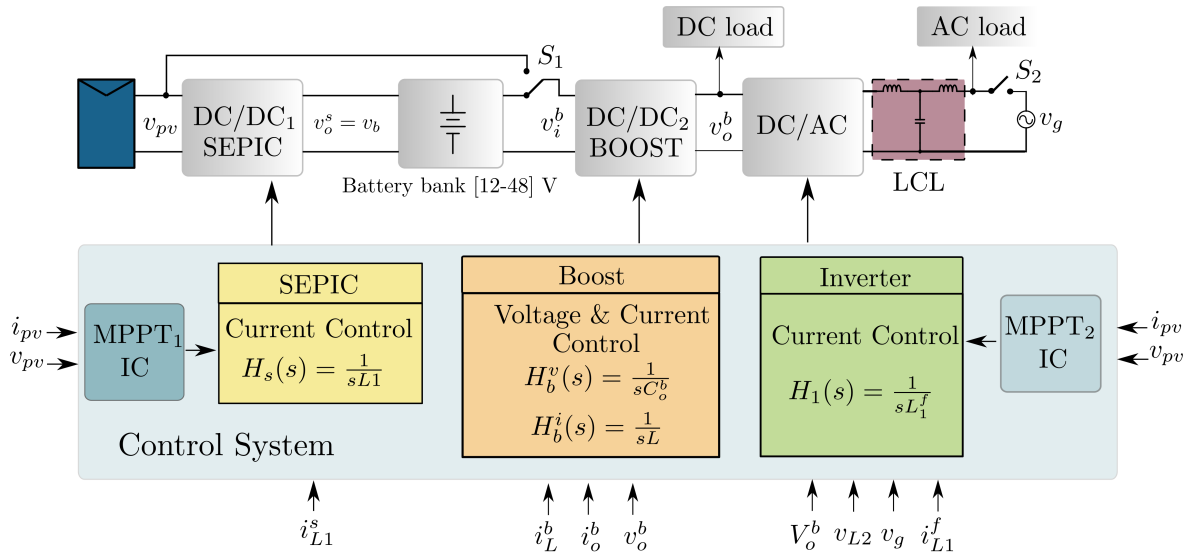


FIGURE 2: Hybrid Multiport Microinverter Topology and Control System.

a wide range with any reference value.

II. TOPOLOGY DESCRIPTION

Figure 2, shows the general topology with the different connection points, the sensing variables, control outputs, and linearized transfer functions of each converter can be seen. The comprehensive control strategy implemented in this work allows systematic to control of the HMM, whether on the DC or AC side of the topology.

The topology is formed by a SEPIC converter, a Boost converter, and a full bridge inverter with an LCL filter for filtering the current injected into the electrical grid. Together with the previously mentioned subsystems, the topology has a battery bank for storing the energy extracted from the PV module. Finally, it is possible to see two switches S_1 and S_2 , whose purpose is to select the operation mode of the HMM.

A. OPERATION MODE

S_1 allows selecting if the energy is sent directly to the DC/DC₂ input or sent to the battery through the SEPIC converter.

This makes it possible to increase the efficiency, thanks to the SEPIC turn-off when the battery bank is fully charged. The DC/DC₁ is a SEPIC converter, where the main characteristic is the capability of step-up and step-down of the output voltage without changing the voltage polarity as with the Buck-Boost converter [23]. In this way, it is possible to connect a battery bank with standard voltage (12 to 48 V), which allows the connection of PV panels with different voltages in the maximum power point. Meanwhile, the On and Off grid operation modes are controlled by switch S_2 , achieving the flexibility to operate under different conditions. To sustain the topology proposal, the next sections will detail the model and control of DC and AC converters.

III. DC CONVERTERS MODELLED AND CONTROLLED BY DOUBLY LINEARIZED LOOPS

Firstly, it is important to highlight that the given explanation in this paragraph is applied to both SEPIC and Boost converters. The control strategy consists of two cascaded control loops, the internal loop controls the current and the external loop allows control of the output voltage. Both loops are modeled and controlled by exact linearization, with the difference that in the external loop it is necessary to apply a power balance strategy. In both cases, the transfer function obtained is an integrator, which will be presented in the analysis below. The circuit schematics for both converters are presented in Figure 3.

The equation that describes the inductor current i_{L1}^s for both commutation states, is:

$$L_1 \frac{di_{L1}^s}{dt} = v_{pv} d_s - v_o^s (1 - d_s). \quad (1)$$

Defining the new input control as:

$$u_c^s = L_1 \frac{di_{L1}^s}{dt}, \quad (2)$$

then replacing u_c^s and solving d_s :

$$d_s = \frac{u_c^s + v_o^s}{v_{pv} + v_o^s}. \quad (3)$$

Equation ((3)) is the obtained linearized equation, and this will be the new input to the system. Output d_s is the modulator signal and it is compared with the carrier triangular signal to generate the control pulse applied to the power MOSFET, as is possible to see in Figure 4.

A. SEPIC EXTERNAL VOLTAGE CONTROL LOOP AND COMPLETE SYSTEM MODEL

For this loop, it is necessary to apply the exact linearization technique together with a power balance strategy; therefore, the input power is equal to the output power, as it is shown in Equation 4:

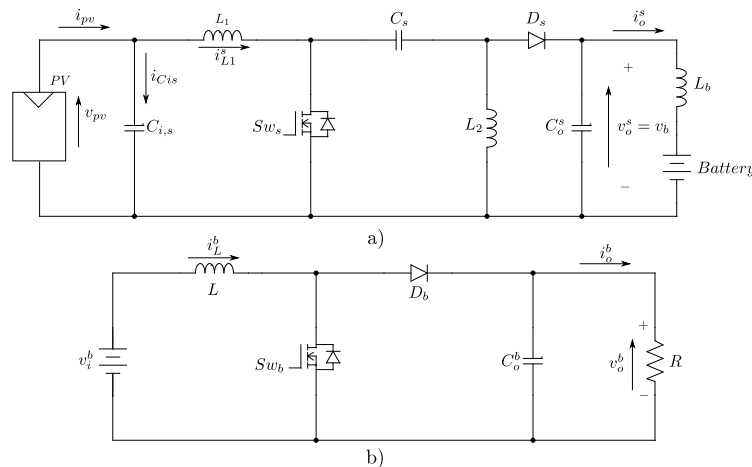


FIGURE 3: DC/DC converter used. a) SEPIC converter, b) Boost converter.

$$v_i^s i_{L1}^s = \frac{1}{2} C_o^s \frac{du_o^s}{dt} + v_o^s i_o^s, \quad (4)$$

where $u_o^s = (v_o^s)^2$. Solving for $C_o^s \frac{du_o^s}{dt}$:

$$C_o^s \frac{du_o^s}{dt} = 2(v_i^s i_{L1}^s - v_o^s i_o^s). \quad (5)$$

The next step is to define the new loop variable for the external loop, as:

$$u_{cs}^e = C_o^s \frac{du_o^s}{dt}. \quad (6)$$

Finally, it is necessary to solve the reference current for the internal loop i_{L1}^s .

$$i_{L,ref}^s = i_L^s = \frac{u_{cs}^e + 2v_o^s i_o^s}{2v_i^s}. \quad (7)$$

This Equation (7) considers that the internal current control loop is at least ten times faster than the voltage control loop; thus $i_{L1}^s = i_{L1,ref}^s$. Figure 4 shows a simplified control block for the output voltage control. The representative transfer function of the linearized model is $1/sC_o^s$. On the other hand, Figure 4 (b) presents the detailed control block with the linearization scheme in the internal and external loop.

Finally, it is necessary to highlight that the external control loop produces the current reference $i_{L1,ref}^s$ to the internal loop.

B. BOOST CONVERTER INTERNAL CURRENT LOOP

As for the SEPIC converter, it is necessary to have the unifying differential equation that models the current inductor i_L^b .

$$L \frac{di_L^b}{dt} = v_i^b - v_o^b(1 - d_b). \quad (8)$$

Defining the new input control as:

$$u_c^b = L \frac{di_L^b}{dt} \quad (9)$$

then replacing u_c^b and solving d_b :

$$d_b = \frac{u_c^b - v_i^b + v_o^b}{v_o^b}. \quad (10)$$

From Equation 10, it is obtained the modulator for generating the Boost converter control signal applied to the power switch is obtained.

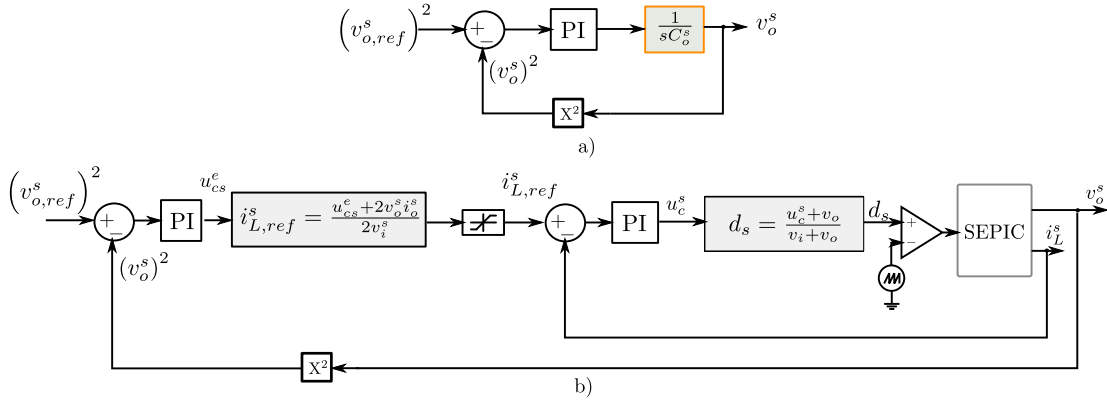


FIGURE 4: SEPIC converter model and control loop. a) simplified, b) detailed.

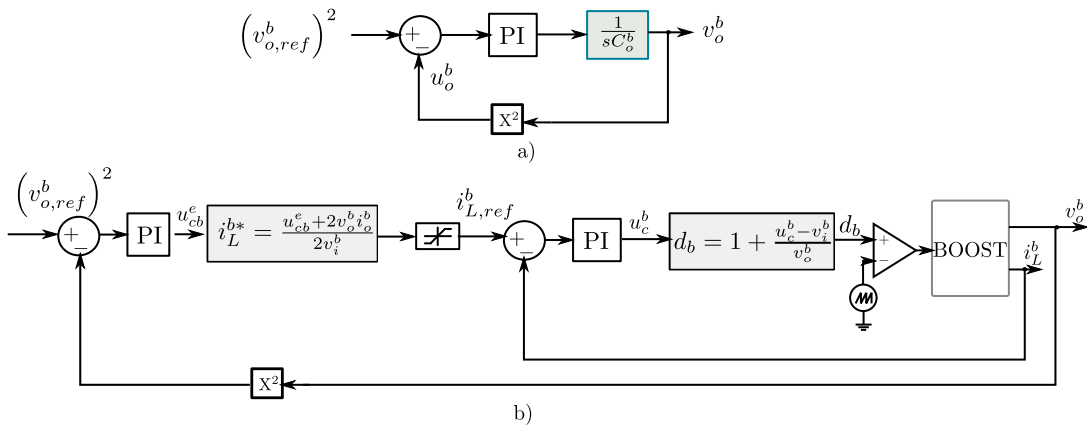


FIGURE 5: Boost converter model and control loop. a) simplified, b) detailed.

C. BOOST, EXTERNAL VOLTAGE CONTROL LOOP, AND COMPLETE SYSTEM MODEL

The power balance and exact linearization technique are used as with the SEPIC converter, obtaining the result that both linearization blocks are equal since both power converter topologies have similar input and output. Therefore, Equation (11) makes it possible to obtain the integrator transfer function $H_b(s) = 1/sC_o^b$. Figure 5 shows the simplified and detailed model, where it is possible to emphasize, the difference between the internal loop and the external loop equality concerning the SEPIC converter.

$$i_L^b = \frac{u_{cb}^e + 2v_o^b i_o^b}{2v_i^b} \quad (11)$$

assuming that $i_{L,ref}^b = i_L^b$, where the inner loop is at least 10 times faster than the external loop.

It is important to note that in both control strategies it is possible to observe in Figures 4 and 5 a current limiter, for the converters, protection, as shown in Figures 4 and 5.

D. MODEL AND CONTROL OF A DC/AC CONVERTER BY EXACT LINEARIZATION

The DC/AC implemented topology in this work is a full bridge single phase inverter, with an LCL filter [24] injected into the electric grid for improving the current quality. The benefits of this filter are size reduction and better current ripple attenuation compared to an L and LC filter [25].

Table 1 presents a comparison of the LCL filter against the L and LC filters [26]–[29], highlighting of the LCL filter. Despite the fact that the number of components is greater in an LCL filter, it exhibits better performance in terms of size, ripple attenuation, and cost. One potential issue with LCL filters is the possibility of resonance, which can complicate the dynamic model of the system. In this work, this issue is addressed by implementing a modulation technique that concentrates the spectrum of switching harmonics. Specifically, the exact linearization technique enables to consider the LCL filter as a simple integrator.

The standards IEEE 519 [30] and IEEE 1547 [31], recommended Practices and Requirements for Harmonics Control in Electrical Power Systems and Standard for Interconnecting Distributed Resources with Electric Power Systems, respectively. The transfer function that relates the current on the inductor L_2^f for the converter voltage v_c is:

$$H_2(s) = \frac{i_{L_2}^f(s)}{v_c(s)} = \frac{1}{s^3 C L_1 L_2 + s(L_1 + L_2)}. \quad (12)$$

Therefore, it is a third-order system, which implies the existence of resonance. This phenomenon is not desired, since it generates problems over the stability and reliability of power electronic converters.

The DC/AC stage control is developed by a Proportional Resonant controller (PR). The strategy consists of the current control injected into the electrical grid in an indirect form

[32]. In other words, the current controlled $i_{L_1}^f$, is the inverter side current. Otherwise, the direct form implies the $i_{L_2}^f$ control or grid side current. The reason for this choice is that indirect control is simpler and does not have the presence of resonance as in the case of direct control. Figure 6 shows the characteristic bode diagrams, where it is possible to see the direct transfer function bode diagram (third order) and the bode for the transfers function that will be obtained with the linearization method.

The objective of this stage is to find the block that allows the means of obtaining the model of the linearized converter-filter (Figure 7) for controlling the current $i_{L_1}^f$. For this purpose, Kirchhoff's voltage law is first applied on the AC side, therefore, it is established that:

$$v_c = L_1^f \frac{di_{L_1}^f}{dt} + L_2^f \frac{di_{L_2}^f}{dt} + v_g \quad (13)$$

The relationship between the voltage V_{dc} and the converter voltage v_c is given by the modulator m .

$$v_c = mV_{dc}. \quad (14)$$

Then, replacing and solving for $i_{L_1}^f$:

$$L_1^f \frac{di_{L_1}^f}{dt} = mV_{dc} - v_{L_2}^f - v_g. \quad (15)$$

Then a new control variable u_c^f must be defined, as:

$$u_c^f = L_1^f \frac{di_{L_1}^f}{dt}, \quad (16)$$

therefore:

$$u_c^f = mV_{dc} - v_{L_2}^f - v_g. \quad (17)$$

Then, solving the modulator m , the linearization block is obtained:

$$m = \frac{u_c^f + v_{L_2}^f + v_g}{V_{dc}} \quad (18)$$

The modulator m is compared with the triangular carrier signal in a unipolar modulation strategy. In this way the triggers of the switches are generated. In conclusion, the described linearization process allows the integrator (Equation (19)) for controlling the energy injected into the electrical grid to be obtained.

$$H_1(s) = H_f(s) = \frac{1}{sL_1^f} \quad (19)$$

TABLE 1: Filter type comparison

Characteristics	L	LC	LCL
Size-Weight	High	High	Low
Ripple Attenuation	Low	Medium	High
Cost	High	Medium	Low

E. SINGLE PHASE PLL

For the energy injection, it is essential to have a PLL algorithm for knowing the electrical grid phase angle. In this work, a digital synchronizer presented in [33], [34] is used, whose operation consists of modifying the sampling time to always achieve the N samples per period regardless of the u_g signal frequency. The control block is presented in Figure 8.

F. PR CONTROL

To handle sinusoidal references, techniques such as control in the dq plane [35], $\alpha\beta$ plane [36], predictive control [37] or Proportional Resonant control [12] can be used. In this work, the last one is selected, given the simplicity and robustness presented for the control of DC/AC converters. The PR control comes from the transformation of the PI control into an AC compensator at the fundamental frequency. Therefore, this control operates in a stationary frame without requiring a transformation such as the dq transformation. The integral action of the PI control is replaced by the transformation:

$$\frac{1}{s} \Rightarrow \frac{2s}{s^2 + \omega_o^2}. \quad (20)$$

Therefore, the resonant proportional control is:

$$C_{RE}(s) = K_p + \frac{2k_i s}{s^2 + \omega_o^2}, \quad (21)$$

where ω_o is the electrical grid frequency.

Figure 9 a), presents the simplified control scheme, where it is possible to observe the PR controller and the resulting transfer function from the application of the exact linearization, whereas, 9 b) details the control scheme detailed for the practical implementation.

IV. MAXIMUM POWER POINT TRACKING ALGORITHM

Two types of MPPT are necessary to implement for the HMM operation. While one of the MPPTs delivers the reference to the SEPIC converter, the second MPPT is responsible for delivering the current reference to be injected into the electrical grid through the microinverter.

Several papers, including [38], highlight the advantages of current control when implementing maximum power point tracking (MPPT) algorithms in a DC/DC converter. Other papers, such as [39] and [40], present implementations where the MPPT algorithm's reference signal is directly applied to the current control system of the electrical grid. In this work, the IC algorithm was operated at a sampling frequency of 100 Hz with a current step of 0.1 A. The current sensors used in the prototype have a bandwidth of 200 kHz.

Although the IC algorithm has been widely used in microinverters and inverters connected to photovoltaic modules, it has been shown that it does not always ensure the selection of the GMPP [41], [42]. However, this work aims to address the challenges of partial shading using an innovative approach based on microinverters, which allows each photovoltaic module to operate independently and minimize the effects of partial shading.

As can be seen in Figure 10 a), the MPPT that allows energy storage in the battery, the algorithm output corresponds to the reference current of the inductor i_{L1}^s , thus, the current injected into the battery is indirectly controlled. Therefore, the internal linearized current loop obtained in the SEPIC modeling subsection is used to work together with the incremental conductance (IC) algorithm.

On the other hand, Akagi's theory [43] indicates that the instantaneous power is:

$$P = \frac{3}{2} (V_d I_d + V_q I_q), \quad (22)$$

where d and q are the subscripts for direct and quadrature, respectively. When the current is in phase with the voltage, it implies that the Equation (22) becomes:

$$P = \frac{3}{2} V_d I_d. \quad (23)$$

Therefore, Equation (23) is employed when the dq transformation is synchronized with the grid voltage. In this context, Figure 10 b) shows the control scheme for monitoring the MPP, where the algorithm will deliver the current I_d as a reference. This magnitude is multiplied by the sine of

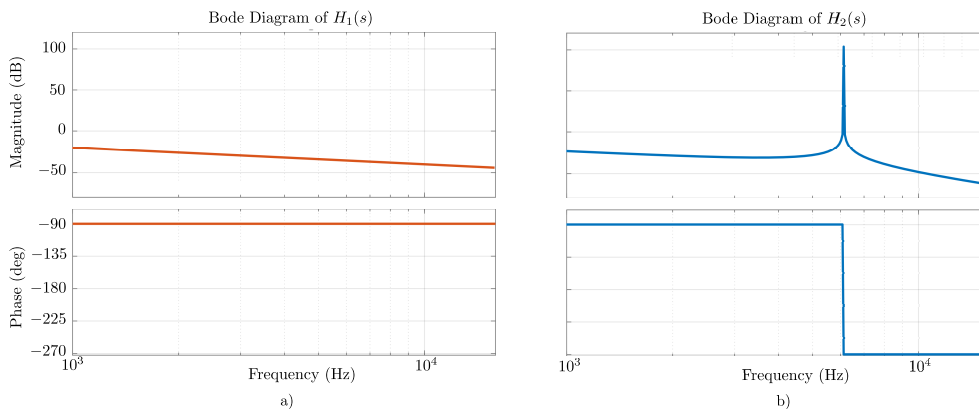


FIGURE 6: LCL Bode diagram. $H_1(s) = i_{L1}^f/u_c^f$ and $H_2(s) = i_{L2}^f/v_c$.

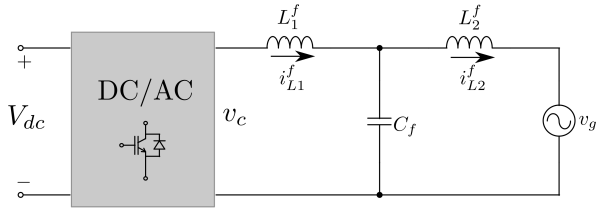


FIGURE 7: Full bridge inverter topology with LCL filter.

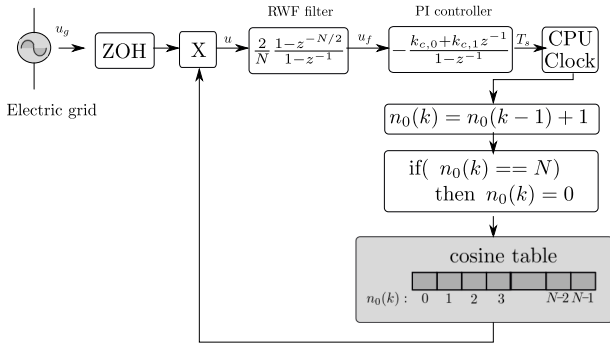


FIGURE 8: Digital Synchronizer Control Block.

the angle obtained from the digital synchronizer. Voltage V_d corresponds to the DC link voltage that feeds the full bridge inverter. This voltage V_d is controlled by the Boost converter and both sub-converters are decoupled. Therefore, the voltage and current are controlled, maximizing the energy extraction. The DC controller (for both Boost or SEPIC) is responsible for maintaining the input voltage inverter on the desired reference value, regardless of the current injected into the electrical grid.

In this work, the incremental conductance algorithm is used with an algorithm modification given the i_{L1}^s current reference, for the SEPIC case, and the i_{L1}^f inverter current reference, as mentioned above. Figure 11 details the algorithm flowchart.

V. EXPERIMENTAL RESULTS

A. SETUP

Figure 12 shows the topology setup, conformed by the SEPIC, Boost, and LCL inverter. For controlling, STM32F103c and STM32F407, microcontrollers are used. As for power supply, the photovoltaic emulator and DC source model 62020H-150S from Chroma are used. While the loads are a 200 Ω - 100 W resistor and the Rigol DL3021 programmable DC electronic load.

B. CONVERTER AND CONTROLLER PARAMETERS

On the DC converters model analysis, it was found that the internal and external transfer function consisted of an integrator in both cases. Similarly, as for the DC/AC stage. Therefore, in theory with only a P controller, it is enough for a DC converter, nevertheless in a practice case inductor and the capacitor has parasitic component. To deal with this

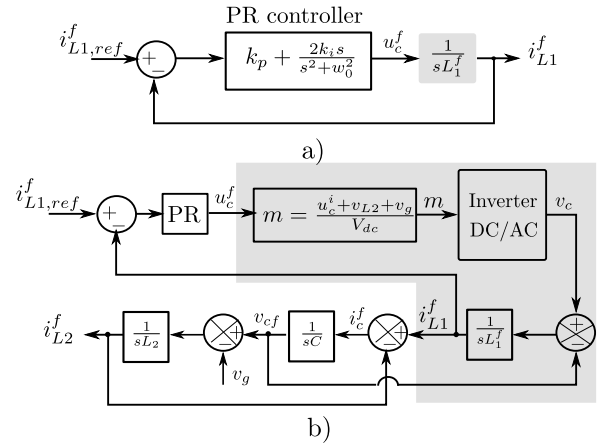


FIGURE 9: Control scheme with exact linearization of the LCL inverter.

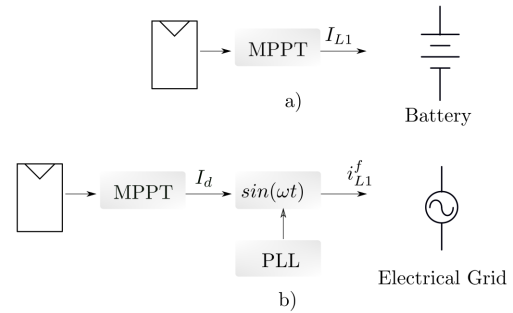


FIGURE 10: MPPTs schemes, a) for energy storage, b) for energy injection to the electrical grid.

TABLE 2: Topology parameters.

Parameter	SEPIC	Boost	INVERTER + LCL
k_p Voltage loop	0.3	0.25	-
T_i Voltage loop	1	1	-
k_p Current loop	20	20	-
T_i Current loop	1	2	-
L	-	2 mH	-
C	-	1000 μ F	-
L_1	2 mH	-	-
L_2	2 mH	-	-
C_s	1 μ F	-	-
k_p	-	-	12
k_i	-	-	1000
L_1^f	-	-	2 mH
L_2^f	-	-	1 mH
c_f	-	-	2 μ F

problem, a PI controller is necessary to achieve zero error in a steady state.

The topology parameters and their controllers are presented in Table 2. The controllers are synthesized by the classical technique of controller design using bode plots.

C. MPPT IMPLEMENTED ON A SEPIC CONVERTER

This subsection aims to present the performance in the energy extraction stage of the PV module. For such a case, the

SEPIC converter is used with the linearized current loop. As it was mentioned, the SEPIC converter current reference i_{L1}^s is provided by the incremental conductance algorithm. Therefore, energy extraction with the MPPT algorithm with output current reference is tested, being detailed in Figure 13. It is important to highlight the inductor current i_{L1}^s , which, as can be seen, does not fluctuate, being this a fundamental characteristic of the IC algorithm. In the first instance, the simulation shows an MPP of 60 Wp (Watt Peak), then at 0.2 s an irradiation step change from 1000 to 900 W/m² is made. At 0.3 s, a step change in temperature was introduced. The results show that the system can maintain optimal performance even when subjected to sudden changes in irradiance and temperature, highlighting its robustness and reliability. Additionally, Figure 13 shows the current and voltage of the PV module.

Experimental results come to validate the proposed strategy, as presented in Figure 14 presented. In this case, a 64 Wp is extracted. As it is possible to observe, the photovoltaic current remains without oscillations when the MPP is found. The current is 4 A and the voltage is 16 V.

In order to present the current control behavior, Figure 15 shows the steady state, where it is possible to see the control of 4 A and 0.2 A current ripple for a 100 kHz switching frequency.

D. BOOST CONVERTER

1) Supplying a DC Load with the Battery Bank as Input Voltage to the Boost Converter.

The Boost converter allows different voltage supplies, where the operating range is from 12 to 100 V at the input. This is possible because the linearized control senses the voltage, and it includes this value in its linearization block. Therefore, the supply can be a battery bank or a PV panel with an open-circuit voltage of around 50 V. In this case, S_1 is in the normal position, where the battery is charged. Figure 16 shows the simulation control, where a voltage step change is made, from 100 to 150 V. The load connected is a 200 Ω resistor. The inductor current is presented, where the time to achieve the current reference value is 2 ms. At the same time, it is possible to see the current limiter performance, around 25 A to protect the power converter. The time to reach the voltage reference value is 20 ms. This is validated with experimental results presented in Figure 17, highlighting the similarity between simulation and experimentation, even during the initialization process, from 0 to 100 V.

2) Supplying a DC Load, with Energy from the PV Emulator as Input to the Boost Converter.

In this case, the Boost is supplied using a PV emulator to test the performance. Therefore, Switch S_1 is changed and the PV energy passes directly to the Boost converter. Figure 18 presents the experimental results for this case, where the voltage output is controlled, with a reference of 100 V. The time to reach the steady state is 100 ms approximately. It

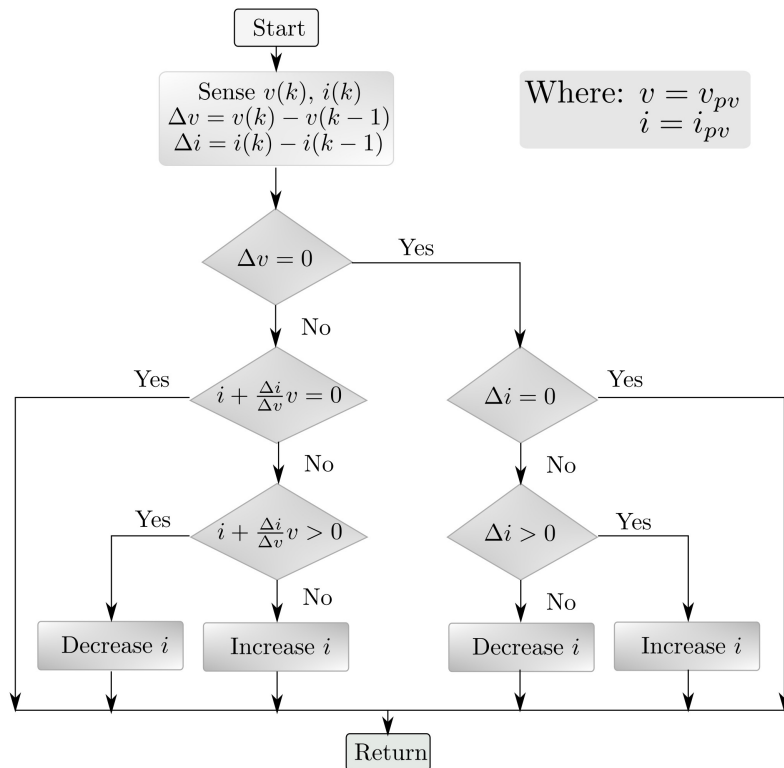


FIGURE 11: Incremental conductance adapted.

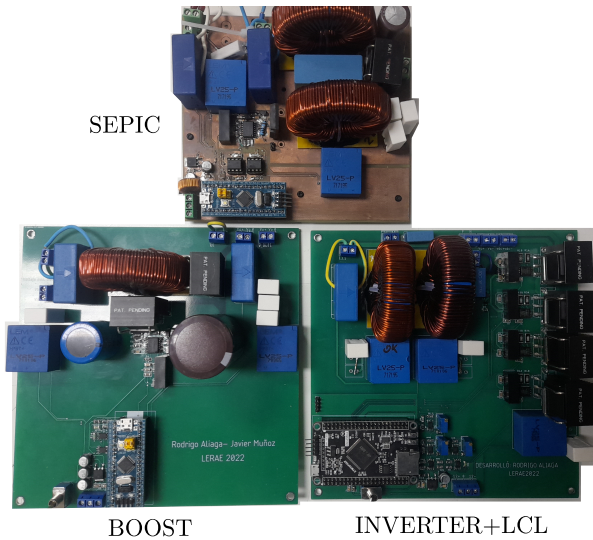


FIGURE 12: Setup

is also possible to see the voltage and current of the PV emulator. The PV power curve shows a 60 Wp, and the output load connected to the Boost converter is a 200 Ω resistor, therefore the output power is 50 W. All this is validated with the PV emulator interface, as can be observed at the top of Figure 18.

3) Input Voltage Variation Tests

An input voltage step change is developed in order to evaluate the control strategy performance. Figure 19 (a) shows a positive step change from 30 to 60 V and Figure 19 (b) a negative step change from 60 to 30 V. In both cases, it is not possible to notice any output voltage variation, thanks to the great performance of the linearized control.

4) Load Impact

Using the RIGOL electronic load model DL3021L, load impacts are made from 200 Ω , 150 Ω and 100 Ω . It is possible to see in Figure 20 (a) that the load impacts produce minimal distortions in the output voltage, with a negligible transient time.

5) Change in the selected input Supply

S_1 is commuted in order to test the control systems when the operation mode is changed. Waveforms are presented in Figure 20 (b), where it is possible to see that the Boost converter output voltage is maintained as constant around the reference 60 V. From t_0 to t_1 the SEPIC is working at the MPP, at around 60 Wp. Then, from t_1 to t_2 the SEPIC is turned off, and the load only demands 18 W from the PV energy. Finally, from t_2 to t_3 the PV energy is turned off and the Boost converter is supplied by the battery. In this case, the v_{pv} is the output circuit voltage, current i_{pv} is 0 A and the battery current is around 2 A.

E. AC TEST IN AN OFF GRID MODE

The objective of this test is to present the behavior of the control focusing on the AC output when the converter is disconnected from the electrical grid, for which a load of 200 Ω is connected to the output of the LCL filter.

The DC linearized control is in charge of controlling the input voltage of the inverter. The Inverter in the Off grid mode is controlled through an open loop strategy with no influence over the DC link voltage. In other words, a decoupling between the two power converters is achieved.

The results show the proper performance of the controller, with reference to tracking time equal to 30 ms, as shown in Figure 21 (a), where it is possible to see the DC link voltage and the AC voltage peak around 100 V.

F. TESTS WITH THE DC/AC INVERTER INJECTING ENERGY INTO THE ELECTRICAL GRID.

Figure 21 (b) shows the current injection experimental test. A current step change is carried out from 4 to 8 A. As can be seen the linearized control allows an instant response time, less than one electrical grid period. The AC voltage was 40 V peak, reduced by an electrical Variac and Trafo.

Another important test is performed in order to see the DC link performance. This is shown in Figure 21 (c), where, as in the previous case, a step change in the injected current is made. The results show the DC link without distortion when a step change from 2 to 4 A is performed, and the AC voltage is 60 V peak.

Finally, the last test (Figure 21 (d)) which was carried out, shows the microinverter turned on. Additionally, the DC link has a 200 Ω load resistor connected. In this case, a small distortion on the DC Link is possible to observe with a transient time of 40 ms.

G. STEP CHANGE TO THE INVERTER INPUT VOLTAGE

This test consists of the inverter input voltage step change, which was performed with the PV emulator, using the voltage source mode. In the first place, Figure 22 (a) shows a step up voltage, where the input voltage is increased from 40 to 50 V, and the current injected is 1 A, without changes when the step is realized. Whereas Figure 22 (b), details a step down voltage from 50 to 40 V.

H. MICROINVERTER WORKING ON MPP, FIRST CASE

In this case, the energy is extracted from the PV emulator, then the voltage is stepped up to 50 V through the Boost converter, and finally, the AC voltage is made. In Figure 23 (a), it is possible to appreciate the corresponding signals. In the first place, the voltage V_{dc} is shown, with a value of 50 V. The AC current injected has a peak of 2 A. The Voltage and current PV have values of 31 V and 1.3 A respectively. Therefore, for this value, the power on the MPP is 41.5 W, as it is possible to see either in the oscilloscope or in the PV emulator interface.

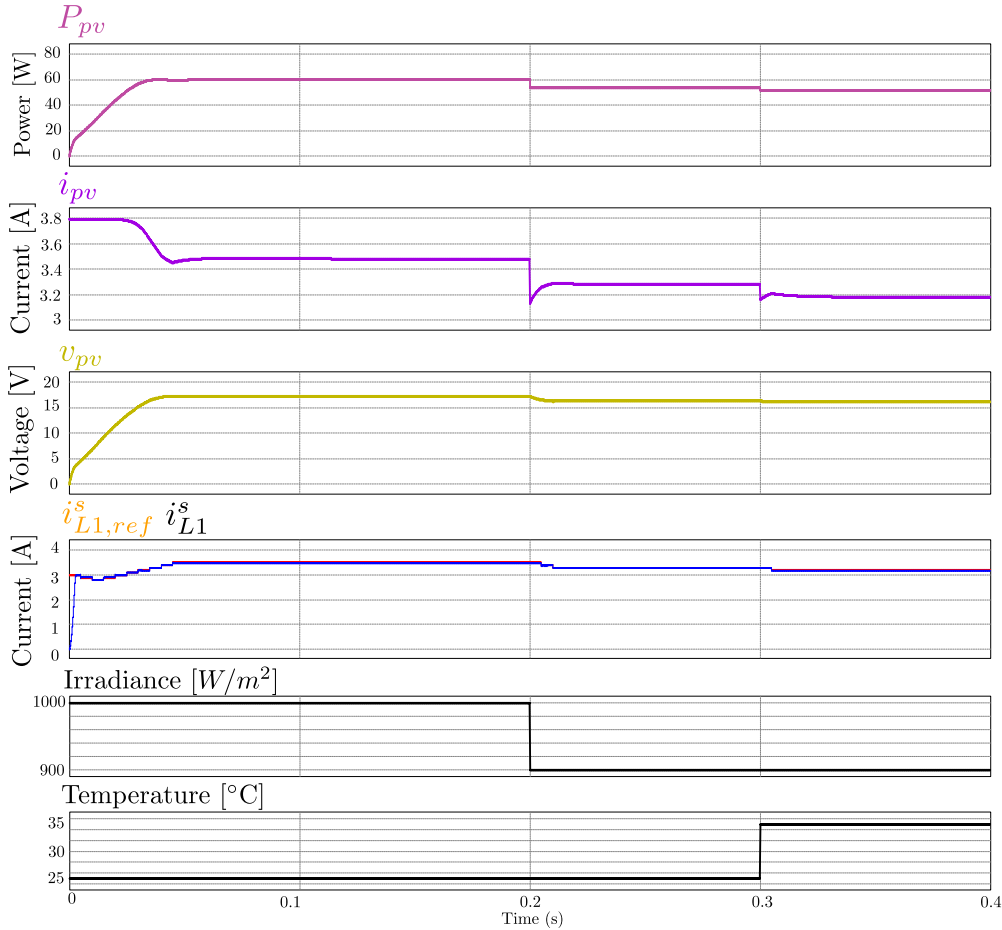


FIGURE 13: Incremental conductance simulation results, with irradiance and temperature step change.

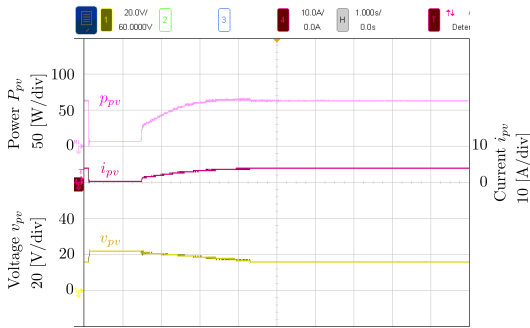


FIGURE 14: Incremental conductance experimental results.

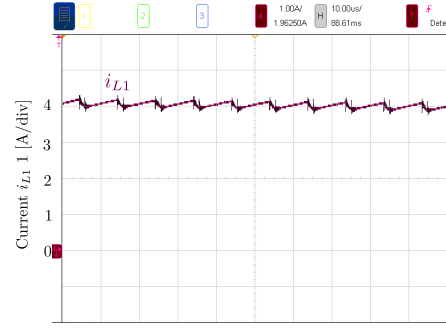


FIGURE 15: Steady state current.

I. MICROINVERTER WORKING ON MPP, SECOND CASE

In this second case, the topology is working on the MPP. The extracted energy is stored in a 12 V battery, then the voltage is stepped up and inverted, the v_{pv} is 17 V, and the i_{pv} is 3.5 A, as seen in Figure 23 (b). It is possible to see a step change in the current injected into the electrical grid from 2 to 4 A.

J. MICROINVERTER, WITH MPPT TURNED ON AND TURNED OFF

The last test which was carried out, consists of the turn on (Figure 23 (C)) and the turn off (Figure 23 (d)), where it is possible to see the correct performance for the current as well as the V_{dc} . At the same time, the MPPT speed is remarkable. Finally, the THD measured was less than 3 % in the tests carried out.

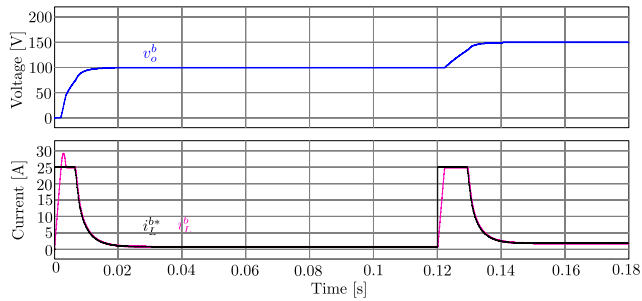


FIGURE 16: Simulation results. Output voltage control, a step change from 100 V to 150 V.

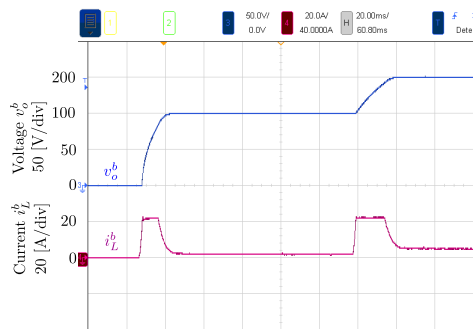


FIGURE 17: Experimental results. Output voltage control, a step change from 100 V to 150 V.

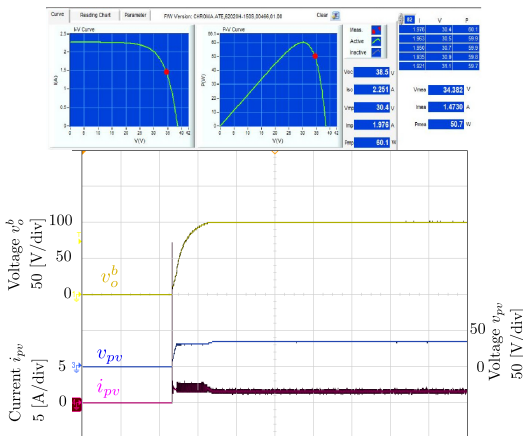


FIGURE 18: Voltage control 100 V, Boost converter supplied by PV emulator.

K. TESTS WITH A WEAK ELECTRICAL GRID.

To test the performance of the current control strategy against a weak grid using exact linearization, a simulation with a grid inductance L_g of 2 mH and a grid resistance R_g of 5 Ω is performed. The results of this simulation are presented in Figure 24, which clearly shows a step change in amplitude from 2 to 4 A peak. This result confirms the effectiveness of the control strategy in accurately following the current reference, even in challenging conditions.

VI. CONCLUSIONS

This paper detailed the modeling and control implementation on the different stages in a hybrid multiport microinverter, with off and on grid operation, plus the DC loads connection capability and battery energy storage to extract and process photovoltaic energy.

Through the exact linearization technique, power electronics converters can be modeled and controlled. As it was demonstrated, a highly nonlinear system can be transformed into a simple linear equivalent system with an integrator as a representative transfer function. The technique is validated through simulation and experimental implementation, both in the DC/DC converters and in the DC/AC stage. By means of PI and PR, the DC/DC and DC/AC conversion stages can be controlled.

Regarding solar photovoltaic energy extraction, an incremental conductance algorithm with a current as output reference is carried out. Simulation and experimental results allow validation the correct performance of the proposed strategy.

The proposed linearization technique with power balance, validated by simulation and experiments, allows control of the cascade control loop. It is verified that the experimental error due to the difference between the model and system is minimal. Furthermore, the experimental results support the correct functioning of the proposed topology.

It is important to highlight the contribution of this paper to simplify and systematize the use of the exact linearization technique in different converters, opening the way to modeling and controlling, both existing converters as well as new topologies that will be developed in the future.

Finally, it should be noted that photovoltaic modules are becoming more efficient, which translates into a higher maximum output power, with some models capable of producing more than 500 Wp. This is especially attractive for home use, where space constraints can limit the number of modules that can be installed, making efficient use of energy even more important.

ACKNOWLEDGMENT

The authors thank to ANID Fondecyt Regular Research Project 1220556, Fondap Solar Energy Research Center N°15110019, ANID CLIMAT AMSUD 210001, ANID - ATE220023 and the Direction of Research of the University of Talca.

REFERENCES

- [1] H. Ziar, S. Mansourpour, E. Afjei, and M. Kazemi. Bypass diode characteristic effect on the behavior of solar pv array at shadow condition. In 2012 3rd Power Electronics and Drive Systems Technology (PEDSTC), pages 229–233, 2012.
- [2] Filippo Spertino, Jawad Ahmad, Alessandro Ciocia, Paolo di Leo, Ali Faisal Murtaza, and Marcello Chiaberge. Capacitor charging method for i-v curve tracer and mppt in photovoltaic systems. Solar Energy, 119:461–473, 2015.
- [3] M M Rahman, M Hasanuzzaman, and N A Rahim. Temperature effect of photovoltaic module under partial shading operation condition. In 3rd IET International Conference on Clean Energy and Technology (CEAT) 2014, pages 1–6, 2014.

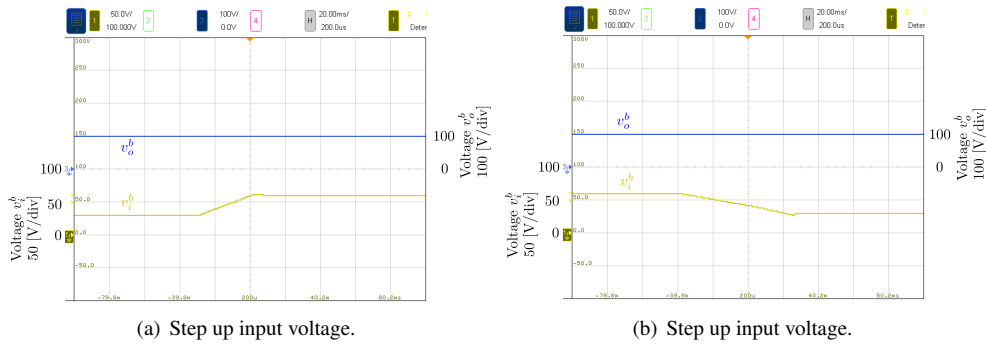


FIGURE 19: Output voltage control for input voltage step changes.

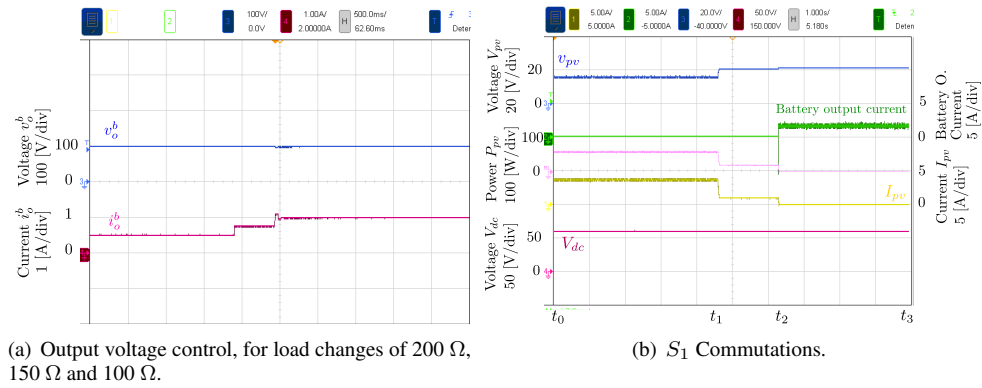


FIGURE 20: DC test.

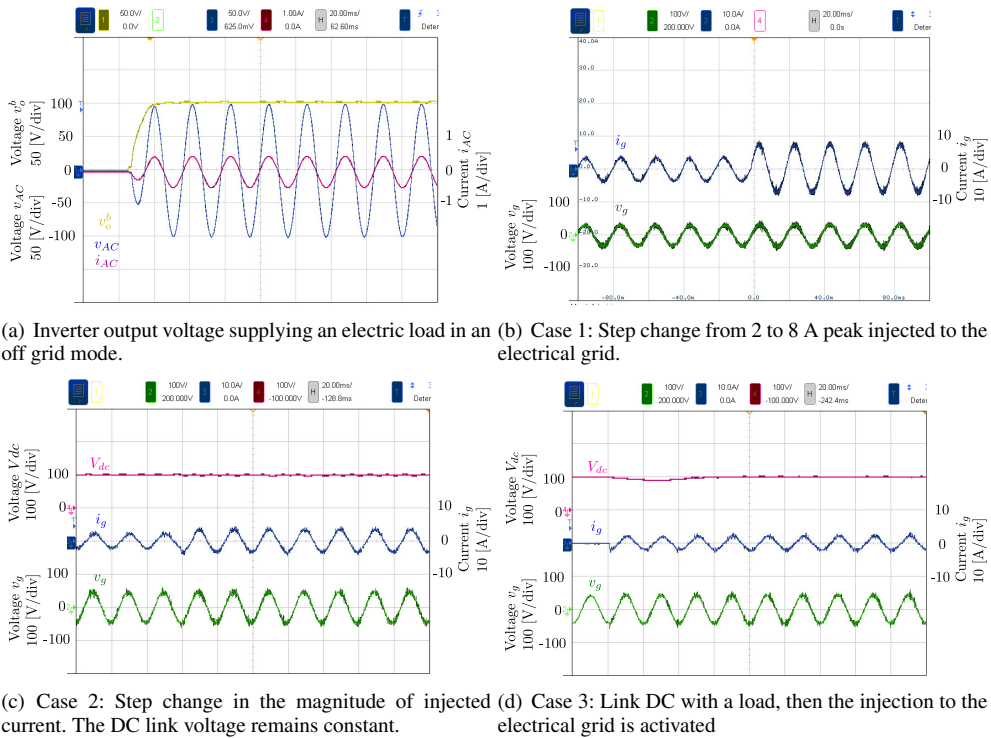


FIGURE 21: AC test.

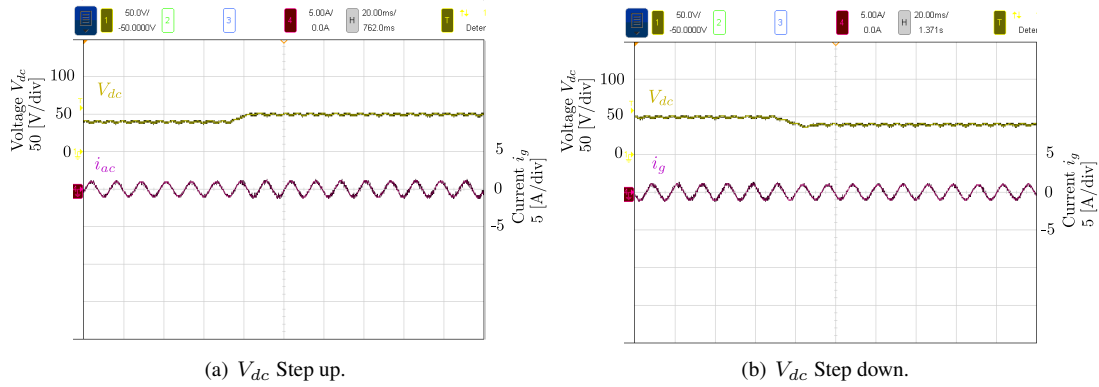


FIGURE 22: V_{dc} step change.

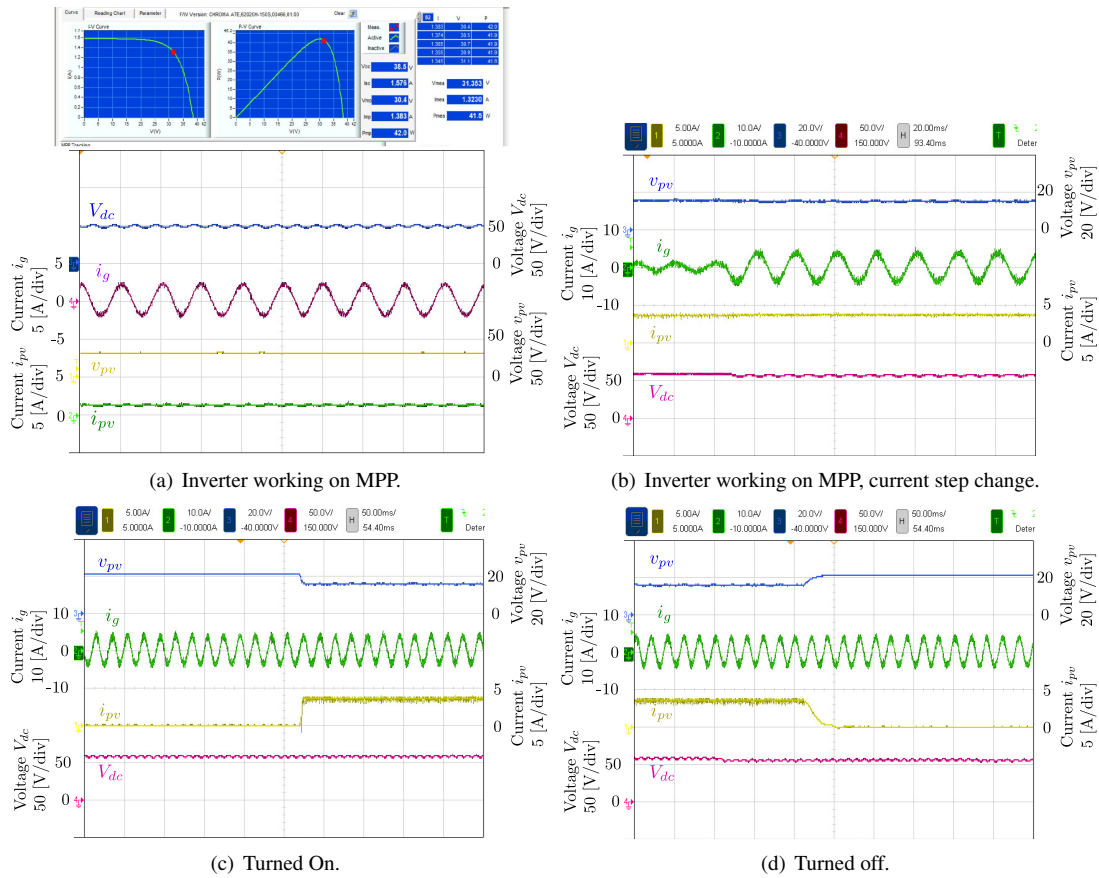


FIGURE 23: MPPT test.

- [4] Kais Abdulmawjood, Samer Alsadi, Shady S. Refaat, and Walid G. Morsi. Characteristic study of solar photovoltaic array under different partial shading conditions. *IEEE Access*, 10:6856–6866, 2022.
- [5] Ratnakar Babu Bollipo, Suresh Mikkili, and Praveen Kumar Bonthagorla. Hybrid, optimal, intelligent and classical pv mppt techniques: A review. *CSEE Journal of Power and Energy Systems*, 7(1):9–33, 2021.
- [6] Radoslaw Kot, Sebastian Stynski, and Mariusz Malinowski. Hardware methods for detecting global maximum power point in a pv power plant. In *2015 IEEE International Conference on Industrial Technology (ICIT)*, pages 2907–2914, 2015.
- [7] Dong Dong, Mohammed S. Agamy, Maja Harfman-Todorovic, Xiaohu Liu, Luis Garces, Rui Zhou, and Philip Cioffi. A pv residential microinverter with grid-support function: Design, implementation, and field testing. *IEEE Transactions on Industry Applications*, 54(1):469–481, 2018.
- [8] Rasedul Hasan, Waqas Hassan, and Weidong Xiao. Pv microinverter solution for high voltage gain and soft switching. *IEEE Journal of Emerging and Selected Topics in Industrial Electronics*, 3(2):352–361, 2022.
- [9] Khalil Alluhaybi, Issa Batarseh, and Haibing Hu. Comprehensive review and comparison of single-phase grid-tied photovoltaic microinverters. *IEEE Journal of Emerging and Selected Topics in Power Electronics*, 8(2):1310–1329, 2020.
- [10] Hadi Tarzamni, Farhad Panahandeh Esmaeelnia, Farzad Tahami, Mahmud Fotuhi-Firuzabad, Payman Dehghanian, Matti Lehtonen, and Frede Blaabjerg. Reliability assessment of conventional isolated pwm dc-dc

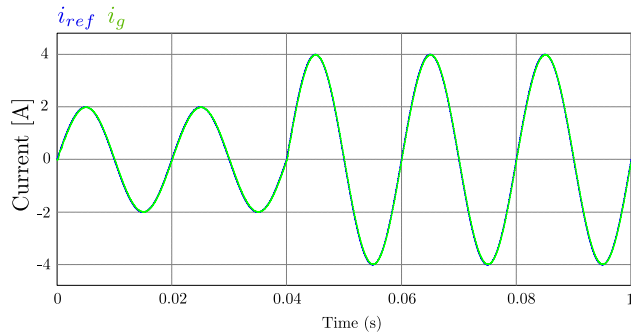


FIGURE 24: Test with a weak grid.

converters. *IEEE Access*, 9:46191–46200, 2021.

[11] Mahajan Sagar Bhaskar, Vigna K. Ramachandaramurthy, Sanjeevikumar Padmanaban, Frede Blaabjerg, Dan M. Ionel, Massimo Mitolo, and Dhafer Almkhles. Survey of dc-dc non-isolated topologies for unidirectional power flow in fuel cell vehicles. *IEEE Access*, 8:178130–178166, 2020.

[12] Blaabjerg Frede. *Control of power electronic converters and systems*. Academic Press, London, 2018.

[13] Chunyang Gu, Hao Yan, Jiajun Yang, Giacomo Sala, Daniele De Gaetano, Xuchen Wang, Alessandro Galassini, Michele Degano, Xin Zhang, and Giampaolo Buticchi. A multiport power conversion system for the more electric aircraft. *IEEE Transactions on Transportation Electrification*, 6(4):1707–1720, 2020.

[14] Jianwu Zeng, Xia Du, and Zhaoxia Yang. A multiport bidirectional dc-dc converter for hybrid renewable energy system integration. *IEEE Transactions on Power Electronics*, 36(11):12281–12291, 2021.

[15] Siyuan Zhou and G.A. Rincon-Mora. A high efficiency, soft switching dc-dc converter with adaptive current-ripple control for portable applications. *IEEE Transactions on Circuits and Systems II: Express Briefs*, 53(4):319–323, 2006.

[16] Jitendra Kumar Singh and Ranjan K Behera. Hysteresis current controllers for grid connected inverter: Review and experimental implementation. In 2018 IEEE International Conference on Power Electronics, Drives and Energy Systems (PEDES), pages 1–6, 2018.

[17] Y. He and F.L. Luo. Study of sliding mode control for dc-dc converters. In 2004 International Conference on Power System Technology, 2004. PowerCon 2004., volume 2, pages 1969–1974 Vol.2, 2004.

[18] Rong-Jong Wai and Li-Chung Shih. Design of voltage tracking control for dc-dc boost converter via total sliding-mode technique. *IEEE Transactions on Industrial Electronics*, 58(6):2502–2511, 2011.

[19] Wassil El Aouni and Louis-A. Dessaint. Real-time implementation of input-state linearization and model predictive control for robust voltage regulation of a dc-dc boost converter. *IEEE Access*, 8:192101–192108, 2020.

[20] Rong-Jong Wai, Meng-Wei Chen, and Yao-Kai Liu. Design of adaptive control and fuzzy neural network control for single-stage boost inverter. *IEEE Transactions on Industrial Electronics*, 62(9):5434–5445, 2015.

[21] Rodrigo Aliaga, Marco Rivera, Patrick Wheeler, Javier Muñoz, Jaime Rohten, Fadia Sebaaly, Ariel Villalón, and Andrew Trentin. Implementation of exact linearization technique for modeling and control of dc/dc converters in rural pv microgrid application. *IEEE Access*, 10:56925–56936, 2022.

[22] C. R. Baier, M. A. Torres, P. Acuna, J. A. Muñoz, P. E. Melín, C. Restrepo, and J. I. Guzman. Analysis and design of a control strategy for tracking sinusoidal references in single-phase grid-connected current-source inverters. *IEEE Transactions on Power Electronics*, 33(1):819–832, 2018.

[23] Niraj Rana, Subrata Banerjee, Santu Kumar Giri, Ashutosh Trivedi, and Sheldon S. Williamson. Modeling, analysis and implementation of an improved interleaved buck-boost converter. *IEEE Transactions on Circuits and Systems II: Express Briefs*, 68(7):2588–2592, 2021.

[24] Weimin Wu, Yuanbin He, Tianhao Tang, and Frede Blaabjerg. A new design method for the passive damped lcl and llcl filter-based single-phase grid-tied inverter. *IEEE Transactions on Industrial Electronics*, 60(10):4339–4350, 2013.

[25] Fei Liu, Xiaoming Zha, Yan Zhou, and Shanxu Duan. Design and research on parameter of lcl filter in three-phase grid-connected inverter. In 2009

IEEE 6th International Power Electronics and Motion Control Conference, pages 2174–2177, 2009.

[26] Utsav P. Yagnik and Mehul D. Solanki. Comparison of l, lc lcl filter for grid connected converter. In 2017 International Conference on Trends in Electronics and Informatics (ICEI), pages 455–458, 2017.

[27] Hanju Cha and Trung-Kien Vu. Comparative analysis of low-pass output filter for single-phase grid-connected photovoltaic inverter. In 2010 Twenty-Fifth Annual IEEE Applied Power Electronics Conference and Exposition (APEC), pages 1659–1665, 2010.

[28] Remus Narcis Beres, Xiongfei Wang, Marco Liserre, Frede Blaabjerg, and Claus Leth Bak. A review of passive power filters for three-phase grid-connected voltage-source converters. *IEEE Journal of Emerging and Selected Topics in Power Electronics*, 4(1):54–69, 2016.

[29] Fei Li, Xing Zhang, Hong Zhu, Haoyuan Li, and Changzhou Yu. An lcl-filter for grid-connected converter: Topology, parameter, and analysis. *IEEE Transactions on Power Electronics*, 30(9):5067–5077, 2015.

[30] Ieee recommended practice and requirements for harmonic control in electric power systems. *IEEE Std 519-2014 (Revision of IEEE Std 519-1992)*, pages 1–29, 2014.

[31] Ieee guide for using ieee std 1547 for interconnection of energy storage distributed energy resources with electric power systems. *IEEE Std 1547.9-2022*, pages 1–87, 2022.

[32] Subhajyoti Mukherjee, Pourya Shamsi, Mehdi Ferdowsi, and Jonathan Kimball. Indirect grid current control of lcl filter based grid-connected converter. In 2019 IEEE Applied Power Electronics Conference and Exposition (APEC), pages 3024–3031, 2019.

[33] Jaime Addin Rohten, Jose Javier Silva, Javier A. Muñoz, Felipe A. Villarroel, David N. Dewar, Marco E. Rivera, and Jose R. Espinoza. A simple self-tuning resonant control approach for power converters connected to micro-grids with distorted voltage conditions. *IEEE Access*, 8:216018–216028, 2020.

[34] Jaime Rohten, José Espinoza, Felipe Villarroel, Javier Muñoz, Pedro Melín, Carlos Baier, and Marcelo Perez. Discrete synchronism methods for polluted single phase and unbalanced three-phase systems. In 2014 IEEE 23rd International Symposium on Industrial Electronics (ISIE), pages 1347–1352, 2014.

[35] Behrooz Bahrani, Alireza Karimi, Benoît Rey, and Alfred Rufer. Decoupled dq-current control of grid-tied voltage source converters using nonparametric models. *IEEE Transactions on Industrial Electronics*, 60(4):1356–1366, 2013.

[36] Yang Han, Zipeng Li, Ping Yang, Congling Wang, Lin Xu, and Josep M. Guerrero. Analysis and design of improved weighted average current control strategy for lcl-type grid-connected inverters. *IEEE Transactions on Energy Conversion*, 32(3):941–952, 2017.

[37] Patricio Cortés, Alan Wilson, Samir Kouro, Jose Rodriguez, and Haitham Abu-Rub. Model predictive control of multilevel cascaded h-bridge inverters. *IEEE Transactions on Industrial Electronics*, 57(8):2691–2699, 2010.

[38] Enrico Bianconi, Javier Calvente, Roberto Giral, Emilio Mamarelis, Giovanni Petrone, Carlos Andrés Ramos-Paja, Giovanni Spagnuolo, and Massimo Vitelli. A fast current-based mppt technique employing sliding mode control. *IEEE Transactions on Industrial Electronics*, 60(3):1168–1178, 2013.

[39] Carlos Muñoz, Marco Rivera, Ariel Villalón, Carlos R. Baier, Javier Muñoz, Roberto O. Ramirez, and Patrick Wheeler. Predictive control with current-based maximum power point-tracking for on-grid photovoltaic applications. *Sustainability*, 13(6), 2021.

[40] Sachin Jain and Vivek Agarwal. New current control based mppt technique for single stage grid connected pv systems. *Energy Conversion and Management*, 48(2):625–644, 2007.

[41] Dezso Sera, Laszlo Mathe, Tamas Kerekes, Sergiu Viorel Spataru, and Remus Teodorescu. On the perturb-and-observe and incremental conductance mppt methods for pv systems. *IEEE Journal of Photovoltaics*, 3(3):1070–1078, 2013.

[42] Md. Wazedur Rahman, Chaitanya Bathina, V. Karthikeyan, and R. Prasanth. Comparative analysis of developed incremental conductance (ic) and perturb observe (po) mppt algorithm for photovoltaic applications. In 2016 10th International Conference on Intelligent Systems and Control (ISCO), pages 1–6, 2016.

[43] Hirofumi Akagi. *Instantaneous Power Theory and Applications to Power Conditioning*. Wiley-IEEE Press, 2007.



RODRIGO ALIAGA received the Eng. degree in mechatronic engineering, and the M.Sc. degrees in energy conversion from the University of Talca, Curicó, Chile, in 2015 and 2017, respectively. He is currently in the process of obtaining his Ph.D. in Engineering Systems.



grid.

JAVIER MUÑOZ received the B.S. degree (Hons.) in electronic engineering and the M.S. and Ph.D. degrees in electrical engineering from the University of Concepcion, Concepcion, Chile, in 2007, 2009, and 2012, respectively. Since 2011, he has been with the University of Talca, Curicó, Chile, where he is currently the Dean of the Faculty of Engineering. His current research and teaching interests include dynamic systems and microinverters for photovoltaic integration to the



MARCO RIVERA received the Electronic Civil Engineering degree and the M.Sc. degree in Engineering, with specialization in Electrical Engineering, from the Universidad de Concepción. Later he obtained the PhD. degree in Electronic Engineering from the Universidad Técnica Federico Santa María, and was awarded with the “Premio Tesis de Doctorado Academia Chilena de Ciencias 2012”, for the best PhD Thesis developed in 2011 for national and foreign students in any exact or natural

sciences program, that is member of the Academia Chilena de Ciencias, Chile. Through the last years, he has been visiting professor at several international universities. He has directed and participated in several projects financed by the National Fund for Scientific and Technological development (Fondo Nacional de Desarrollo Científico y Tecnológico, FONDECYT), the Chilean National Agency for Research and Development (Agencia Nacional de Investigación y Desarrollo, ANID), and the the Paraguayan Program for the Development of Science and Technology (Proyecto Paraguay para el Desarrollo de la Ciencia y Tecnología, PROCENCIA), among others. He has been the responsible researcher of basal financed projects whose objective is to enhance, through substantial and long-term financing, Chile's economic development through excellence and applied research. He has managed several bilateral agreements for the Universidad de Talca with international universities. He is the Director of the Laboratory of Energy Conversion and Power Electronics (Laboratorio de Conversión de Energías y Electrónica de Potencia, LCEEP) and the Technology Center for Energy Conversion (Centro Tecnológico de Conversión de Energía, CTCE). He is full professor at the Department of Electrical Engineering from the Universidad de Talca and his main research areas are matrix converters, predictive and digital controls for high-power drives, four-leg converters, development of highperformance control platforms based on field-programmable gate arrays, renewable energies, advanced control of power converters, design, assembly and start-up of power converters, among others. He has published over 450 academic publications in leading international conferences and journals.



PAT WHEELER received his BEng [Hons] degree in 1990 from the University of Bristol, UK. He received his PhD degree in Electrical Engineering for his work on Matrix Converters from the University of Bristol, UK in 1994. In 1993 he moved to the University of Nottingham and worked as a research assistant in the Department of Electrical and Electronic Engineering. In 1996 he became a Lecturer in the Power Electronics, Machines and Control Group at the University of Nottingham, UK. Since January 2008 he has been a Full Professor in the same research group. He was Head of the Department of Electrical and Electronic Engineering at the University of Nottingham from 2015 to 2018. He is currently the Head of the Power Electronics, Machines and Control Research Group, Global Director of the University of Nottingham's Institute of Aerospace Technology and was the Li Dak Sum Chair Professor in Electrical and Aerospace Engineering. He is a member of the IEEE PELs AdCom and is currently IEEE PELs Vice-President for Technical Operations. He has published over 750 academic publications in leading international conferences and journals.



JAIME ROHTEN received the Engineering degree in Electronic Engineering (with first-class honors), the M.Sc. and D.Sc. degrees in Electrical Engineering from the University of Concepcion, Concepcion, Chile, in 2010, 2012, and 2017, respectively. His research interests include renewable energies, digital nonlinear, resonant, and predictive control for voltage or current source converters. Since 2015, he has been teaching in the areas of power electronic and control systems analysis with the Department of Electrical and Electronic Engineering, Universidad del Bío-Bío, Concepción, Chile.



ANDREW TRENTIN Andrew Trentin received the “Laurea” Master's degree and Ph.D. degree in electrical engineering from the University of Bologna, Bologna, Italy, in 2001 and 2005, respectively. Since 2005, he has been a Research Fellow in the Power Electronics, Machines and Control Research Group, at The University of Nottingham, UK, and promoted to Senior Research Fellow in 2012. His research interests are power electronics and electrical drives for different applications and in direct ac/ac matrix converters.

...